Coexistence of Quantum and 1.6 Tbit/s Classical Data over Fibre-Wireless-Fibre Terminals

Andy Schreier, Obada Alia, Rui Wang, Ravinder Singh, Grahame Faulkner, George Kanellos, Reza Nejabati, Dimitra Simeonidou, John Rarity, and Dominic O'Brien, *Member, IEEE*

***Abstract*—In this paper a fibre free-space fibre link that allows a quantum key distribution (QKD) signal and high-speed data to be transmitted in a single optical beam is presented. This setup has the potential to provide ultra-high data rate secure wireless connectivity within indoor spaces. Both quantum and classical channels were transmitted using wavelengths in the C band, over a range of 2.5 m in free space and in the presence of a 200 lx background illumination. Raman noise caused by the light propagating in the optical fibres which provide connections to the free-space segment, together with geometric loss of the free-space link are the major impairments. Results yield secret key rates of 2.343 kbit/s when the QKD signal is sent without high-speed data (and associated Raman noise), and rates of 1.305 - 1.996 kbit/s when high-speed data is also transmitted (depending on spectral separation of QKD and classical information). Further, it is shown that the secret key rate can be optimised by increasing loss to attenuate the Raman noise by misalignment of the link. Improvement of the secret key rate from 1.305 kbit/s to 1.887 kbit/s was shown using this method.**

***Index Terms*—beamsteering, free-space optical, QKD, quantum communications, quantum key distribution, security.**

I. Introduction

QUANTUM key distribution (QKD) enables the exchange of theoretically secure information, symmetrical keys with the unique ability to detect the presence of eavesdropping third parties [1]. Since the publication of the first QKD protocol in 1984 [1], QKD has been applied in fields of satellite-to-ground communication [2]–[6], fibre communication [7]–[23] and free-space communication [24]–[29]. Quantum links, combined with high data rates classical links [11]–[14] and ultra-long-haul fibre QKD transmissions covering distances of up to 830 km in fibre [16] have been demonstrated. Distributing QKD in dedicated fibre access networks have been proposed in [17]–[19]. The coexistence of QKD with classical communication channels is challenging in fibres due to the high power of the classical channels and the noise created by non-linearities in the fibre, such as Raman scattering, which degrade the QKD performance. Hence, the launch power of classical communication channels [30] and the wavelength spacing between classical and quantum channels [11]–[13] directly affect the QKD performance. Various approaches to coexistence have been reported and include active switching between drop fibres [20], multi-core fibres [14], WDM-PON [21] and GPON [22]. Recently, hollow core fibres demonstrated coexistence with the unique ability to tolerate up to 3 orders of magnitude higher transmission powers of the classical channel compared to standard single mode fibres, making those a promising transmission medium [15].

QKD in free-space applications has been demonstrated with indoor handheld devices [24]–[26] and outdoor drones [27], [28]. Recently, the first lab demonstration of a 2 m free-space transmission of the Coherent One-Way (COW) protocol was published [29]. Free-space QKD systems are typically used over long distance, but the increasing demand for secure in-building connectivity makes short-range free-space QKD attractive. Such short-range links can be achieved by using Fibre-Wireless-Fibre (FWF) terminals [31]–[35] combined with fibre-based QKD systems. Ultra-high data-rate classical links have been achieved using FWF techniques, and the addition of a QKD channel might offer ultra-high rate data communications with the additional security that QKD brings. In this case the impairments are different from all-fibre based systems. Free-space has no nonlinearity at the power levels used, but impairments due to ambient light being detected must be considered [36]. In addition effects due to turbulence need to be assessed [29]. There has been some modelling to suggest that this FWF approach can support indoor QKD systems on their own [37] and in coexistence with classical communication channels [38]. However, experimental data are lacking and experimental characterisation is required.

This paper is organised as follows: Section II describes the design and typical performance of the compact FWF terminals. Section III explains the COW protocol and its implementation as well as presents an experimental characterisation of the transmission of QKD signals through the FWF system. Experimental results on the coexistence of QKD and classical communication channels are detailed in section IV. Conclusions are presented in section V.

II. FWF terminals

The challenge for any FWF systems is maintaining link alignment with high accuracy. For a system that uses single-mode fibre with typical commercial collimators the beam divergence/acceptance angles are $\approx$ 0.05 degrees, so any system must maintain alignment to this tolerance. Systems that use beacon-based tracking [2]–[6] and tracking that uses

A. Schreier, G. Faulkner and D. O'Brien are with the Department of Engineering Science, University of Oxford, United Kingdom, e-mail: ({andy.schreier},{dominic.obrien}@eng.ox.ac.uk).

O. Alia, R. Wang, G. Kanellos, R. Nejabati, D. Simeonidou and J. Rarity are with the Department of Electrical & Electronic Engineering, University of Bristol, United Kingdom.

R. Singh is a former member of University of Oxford and now with the Cambridge Research Laboratory, Toshiba Europe Ltd., CB4 0GZ Cambridge, United Kingdom.

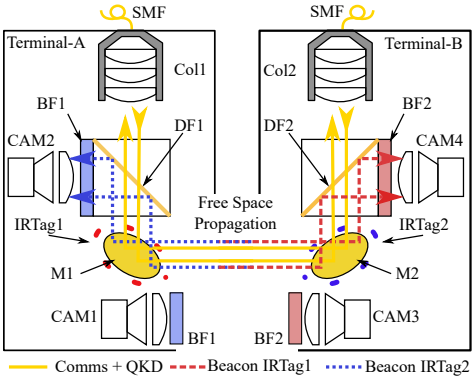

Fig. 1. Schematic of the FWF terminals.

the communications signal [31], [32], [39] have been demonstrated. In this paper a simplified version of such beacon signals will be used to drive the compact FWF terminals [34].

Fig. 1 shows a schematic of the FWF terminals as described in [34]. Light from single-mode fibre (SMF) is fed into the terminals and collimated (Col1 or Col2) before being actively steered using fast steering mirrors (M1 or M2). These dual-axis steering mirrors allow for beam steering with up to $\pm$ 50° optical deflection per axis and a steering resolution of less than 5 μrad. The tracking system controlling M1 & M2 uses infrared (IR) Tags operating at 800 nm and 890 nm as well as a set of cameras. The IR Tags provide localisation beacons, represented by red and blue lines in Fig. 1, respectively. Dichroic beam splitters (DF1 & DF2) separate the localisation beacon light from the combined communication channels. Cameras CAM1 & CAM3 were set up with a wide field of view (FoV) which allows for locating the other terminal, while the cameras (CAM2 & CAM4) have a narrow FoV allowing for high precision tracking. Optical band-pass filters (BF1 & BF2) in front of each camera reject ambient light to enable reliable localisation and tracking of the terminals. The latency of the tracking system supports communications between nomadic operations [34].

The tracking performance of the FWF terminal system was characterised, and shown to achieve a tracking resolution of 0.021° horizontally and 0.014° vertically all within a tracking latency of 216 ms. In operation, the FWF system supported WDM channels transmitting data at 1 Tbit/s transmission rates for nomadic operation [35]. Wavelengths across the O and C band can be transmitted simultaneously [40].

There are two main contributors to the overall insertion loss of the FWF terminal system: (i) geometric loss L_{geo} and (ii) coupling loss induced by angular misalignment L_ϕ. The geometric loss scales with distance between the terminals as the collection area of the optical receiver remains constant whereas the divergence of the transmitted beam causes the illuminated area to grow with the square of the distance. The geometric loss can be expressed in dB by Eq. (1) [41].

$$L_{geo} = 10 \log \left[\frac{4\omega_T^2 \omega_R^2}{\frac{\lambda^2 Z_0^2}{\pi^2 n^2} + (\omega_T^2 + \omega_R^2)^2} \right] \quad (1)$$

where n represents the refractive index of the medium between the two collimators ($n = 1$ is assumed in all calculations presented in this paper), λ the wavelength of light in vacuum, Z_0 is the distance between the two collimators and ω_R and ω_T are the Gaussian beam radii of the receiver collimator and transmitter collimator, respectively.

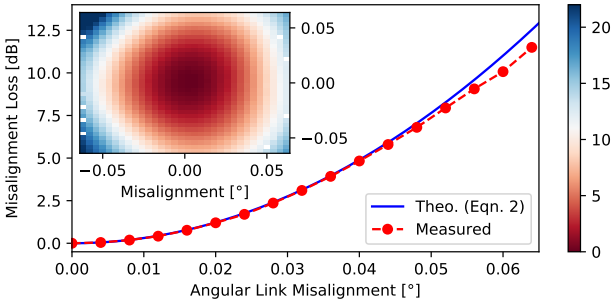

Fig. 2. Average of measured misalignment losses gathered from the inset and a theoretically estimated loss based on Eqn. (2). The inset shows the measured misalignment loss as a function of horizontal and vertical steering angles.

Angular misalignment causes coupling losses due to the limited area in which light is guided in fibres as well as due to the limited acceptance angle of fibres. The angular misalignment loss in dB is given in Eqn. (2) [41]

$$L_\phi = \frac{20}{\ln 10} \frac{\left(\frac{n\pi\omega_R}{\lambda}\right)^2 \left[\left(\frac{\lambda Z_0}{\pi n \omega_T^2}\right)^2 + \left(\frac{\omega_R}{\omega_T}\right)^2 + 1 \right]}{\left(\frac{\lambda Z_0}{\pi n \omega_T^2}\right)^2 + \left[\left(\frac{\omega_R}{\omega_T}\right)^2 + 1 \right]^2} \sin^2 \phi, \quad (2)$$

where ϕ the angular misalignment between the optical axis of transmitter and receiver collimators. Fig. 2 illustrates good agreement between the theoretical estimation and the measured data. In order to verify angular misalignment was the dominant effect in inducing loss the lateral offset caused by mirror misalignment was estimated (knowing the distance between the mirror and the receiver collimator aperture). This was used in Eq.36 of [41] to estimate the loss, and this was significantly smaller than the measured loss, indicating that angular misalignment is the dominant effect for losses at angles less than 0.05°.

III. QKD VIA FWF TERMINALS

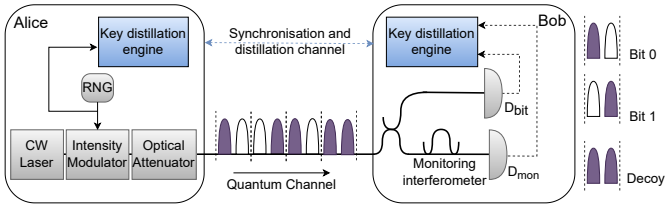

Fig. 3. Illustration of COW protocol principle.

An IDQuantique Clavis3 QKD system was deployed to generate the Qubits for all following experiments [42]. The Clavis3 is a DV-QKD system which implements a Coherent One-Way (COW) protocol based on time-bin Qubits. As

shown in Fig. 3, the COW protocol utilises weak optical coherent pulses and interferometers for detection. As the system is based on time-bin encoding of Qubits and the coherent pulses are propagating in the same spatial mode and separated by a given time, the bases are measured by determining the time of the detection. If the detection occurs in the early time-bin, the Qubit value is considered as $|0\rangle$ state, whereas if the Qubit occurs in the late time-bin, it is considered a $|1\rangle$ state. One of the two Qubit basis (the computational basis) is used to generate the raw keys and the other is used to estimate the security level of the exchanged Qubits in the first basis. The security of the COW protocol is analysed by checking the coherence between two consecutive pulses using the interferometer at the receiver (Bob) station. Therefore, the transmitter (Alice) is required to generate the same phase relation between any two consecutive pulses. To further enhance the security of the COW protocol, a decoy state - consisting of an early and a late optical pulse with the same energy level - is emitted from time to time. The phase between one of the pulses of the decoy state and the consecutive pulses must be identical to the phase between pulses of the computational basis to detect an eavesdropper. Finally, the decoy state and second basis analysis are used to estimate the security level of the raw key rate which is generated by the computational basis [43], [44].

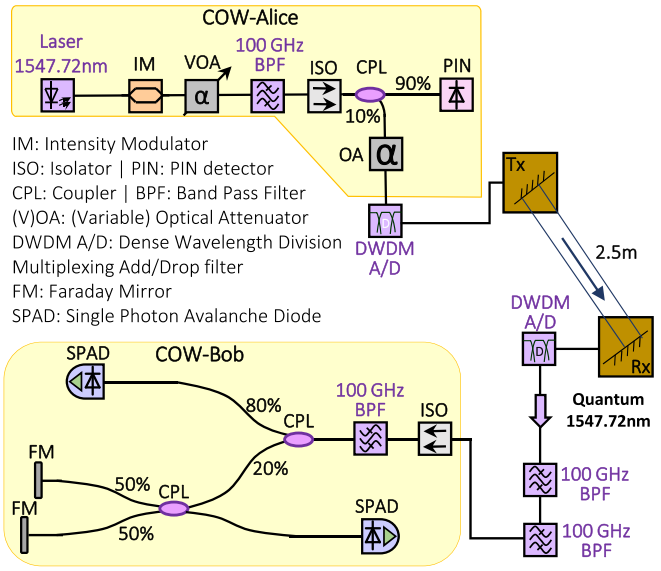

Fig. 4. Experimental testbed for QKD transmission over 2.5 m enabled by FWF terminals.

Fig. 4 shows a schematic overview of the IDQuantique Clavis3 QKD system. The transmitter (Alice) uses a continuous wave (CW) laser at a fixed wavelength (1547.72 nm) providing time positioned weak coherent optical pulses with the aid of the intensity modulator (IM). The weak pulses are attenuated to the appropriated mean photon number value in multiple steps. The variable attenuator (VOA) is set based on the measured power at the output of the PIN monitoring detector at the 90% arm of the 90/10 coupler (CPL). The 10% output is connected to a fixed optical attenuator (OA) that attenuates the light signal to the required intensity level. The 100 GHz bandpass filter (BPF) and the optical isolator (ISO) are included to protect the transmitter from back reflections and to prevent Trojan horse attacks [45].

The receiver (Bob) consists of two branches, the computational basis analyzer branch and the branch checking the phase relation. The branches are separated by a 80/20 coupler as shown in Fig. 4. The computational basis analyzer is connected to the 80% arm and utilises a single-photon detector only. The second branch fed from the 20% output of the coupler, deploys an unbalanced Michelson interferometer with Faraday mirrors (FM) to compensate for any polarization variations. This compensation is crucial to maintain matching polarization modes of the two interferometer beams which recombine in the 50/50 coupler. A single-photon detector is connected on the free output of the interferometer to check the phase relation between consecutive pulses. The optical isolator and 100 GHz bandpass filter are deployed to limit the background noise effects on the detector and to prevent Trojan horse attacks.

Fig. 4 also illustrates the use of additional add/drop filters and bandpass filters used when integrating the FWF terminals. The overall link loss between COW-Alice and COW-Bob was measured to be 11.5 dB of which 6.05 dB are associated with the FWF terminals (placed 2.5 m apart). All following experiments in this paper were conducted within a 200 lx lab environment resulting in ambient light induced count rates of minimum 1.9 kcounts/s to a maximum of 2.3 kcounts/s with a standard deviation of 100 Hz when using a free running IDQ ID210 detector (settings: 5% efficiency, 25 μs dead time and 10 s integration time). The source of ambient light is an LED light spot which has been directed at the receiver FWF terminal. However, diffused light from other light sources can not be excluded but is assumed to be of significantly lesser intensity. The measurement result shows that there is no significant difference between the thermal noise of the detector and the counts induced by ambient light. Hence, the spatial filtering of the receiving terminal and the spectral filtering in place allow for a QKD transmission in a 200 lx lab environment free of any significant penalty to ambient light.

The IR Tags of the FWF terminals also have potential to induce additional counts degrading the QKD performance. Fig. 5a) shows the secret key rate (SKR) and the corresponding quantum bit error rate (QBER) of two hour test runs with and without the IR Tags for an aligned link with fixed mirror positions. Neither the SKR nor the QBER rate has shown any significant sensitivity to the emission of the IR Tags. Photons emitted by the IR Tags (800 nm and 890 nm, respectively) are expected to couple into the fibre path, however, the limited field of view of the fibre and the reduced photon detection efficiencies at those wavelengths minimise the induced counts to a negligible level. Therefore, the tracking system of the FWF terminals has a minimal impact on the QKD performance.

Any free-space system inherently relies on the alignment of Alice and Bob. As shown in Fig. 2 and Eqn. (2), controlling the angular link misalignment is key to providing a stable QKD link as minor changes can cause significant changes in insertion loss. Fig. 5b)-d) illustrate QKD performance

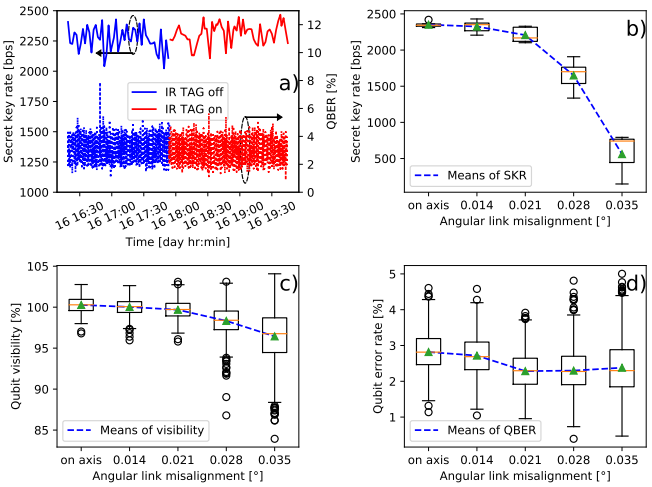

Fig. 5. Characterising the QKD performance . a) Influence of the IR Tag used for localisation and tracking. b)-d) Secret key rate, visibility of Qubits and Qubit error rate plotted against the angular link misalignment of the terminals at a distance of 2.5 m.

key parameter when deliberately steering the receiving FWF terminal off-axis. It can be seen that the SKR and visibility decrease with increasing off-axis angles, whereas the QBER remains almost constant as expected. These results indicate that the angular link misalignment causes increasing insertion loss as well as affecting the Qubit visibility. An angular misalignment of $0.042°$ (insertion loss equivalent of 4.9 dB according to Fig. 2) exceeded the systems margin preventing the IDQuantique Clavis3 system from sifting secret keys. A design with a large enough link budget overhead to tolerate losses induced by fibre optical components as well as the distance and angular misalignment of the terminals is crucial for seamless operation. Thus, the links in all experiments were manually optimised for minimum losses to handle the margins. In any practical environment, the accuracy of the tracking system used in the FWF terminals ($\approx 0.02°$ [34]) needs to be improved for the given distance of 2.5 m. However, the losses can be traded between losses induced by the fibre optical components, the link distance and the maximum angular misalignment / required tracking accuracy.

IV. Coexistence of QKD and Classical Communication Channels via FWF Terminals

Fig. 6 illustrates the experimental system setup used to demonstrate the coexistence of eight classical channels with a DV-QKD channel over a 2.5 m free space enabled by a FWF terminal system. For the classical channels, two optical DWDM platforms are used with bandwidth-variable transponders (BVTs) [46]. Each of these units include four BVT ports and each port can be tuned to any wavelength in the C-band according to the ITU-T 50 GHz grid. All 8 ports of the BVT were configured with a 16-QAM modulation for a transmission rate of 200 Gbit/s per channel resulting in 1.6 Tbit/s of transmission overall. Soft-decision forward error correction (SD-FEC) allowed a 15% error with a detector sensitivity of -23 dBm. Finally, all the ports were configured

TABLE I
Parameters for the Coexistence Testbed

Parameters	Value
Classical Channels	
Number of Channels	8
Classical Channel Frequencies Scenario 1 (Sc1)	193.60 THz, 193.55 THz, 193.50 THz, 193.45 THz, 193.40 THz, 193.35 THz, 193.30 THz, 193.25 THz
Classical Channel Frequencies Scenario 2 (Sc2)	192.60 THz, 192.55 THz, 192.50 THz, 192.45 THz, 192.40 THz, 192.35 THz, 192.30 THz, 192.25 THz
Grid Spacing	50 GHz
Modulation Format	16-QAM
Optical Signal-to-Noise Ratio (OSNR)	30 dB
Transmission rate per Channel	200 Gbit/s
Total transmission rate	1.6 Tbit/s
Pre-FEC Level	15%
Detector sensitivity*	-23 dBm
Quantum Channel	
DV-QKD Wavelength	1547.72 nm
DV-QKD Frequency	193.70 THz
QKD Protocol	COW
Maximum Distance	80 km @ 16 dB loss
Optical Band Pass/Rejection Filter (OBRF)	
Insertion loss band pass port	0.5 dB
Center wavelength band pass port	1547.72 nm
Bandwidth band pass port	100 GHz (0.8 nm)

**Corresponding to 16-QAM Modulation @200 Gbit/s (BER 10^{-3}).*

to match a total power of 0 dBm at the output of the FWF Tx terminal to meet eye safety regulations [47].

As shown in Fig. 6, the eight coherent output ports of the BVT are multiplexed using a wavelength selective switch (WSS) which acts as a band pass filter (BPF) with 30 dB of isolation. Subsequently, the wavelength accumulated signal is filtered. First, by a tuneable band pass filter (TBPF) with a flat-top and sharp filter edges (pink profile in the lower trace of the inset Fig. 6) with a high isolation of 60 dB. Second, a notch filter was deployed to further suppress the noise level at the quantum channel wavelength (1547.72 nm). The filtered signal can be monitored in-situ via a 95/5 coupler (black channels in the inset Fig. 6). The 95% output port of the coupler feeds into a DWDM add/drop (A/D) filter combining the quantum and classical channels which are subsequently fed into the FWF Tx terminal. After a 2.5 m free-space transmission another DWDM add/drop filter is deployed passing the quantum channel through a double stage filtering using two fixed WDM band-pass filters (red profile in the lower trace inset Fig. 6) to eliminate any noise generated by the classical channels and supress ambient light. The output of the filter pack is connected to the Bob-QKD unit. The classical channels are reflected at the DWDM A/D filter and are guided to an optical isolator. The isolator prevents the local oscillator used by the BVT Rx from entering the Bob-QKD unit and therefore interfering with the QKD measurements. Furthermore, the isolator suppresses amplified spontaneous emission (ASE) noise generated by the Erbium-doped fibre amplifier (EDFA) boosting the classical signals to suitable detection

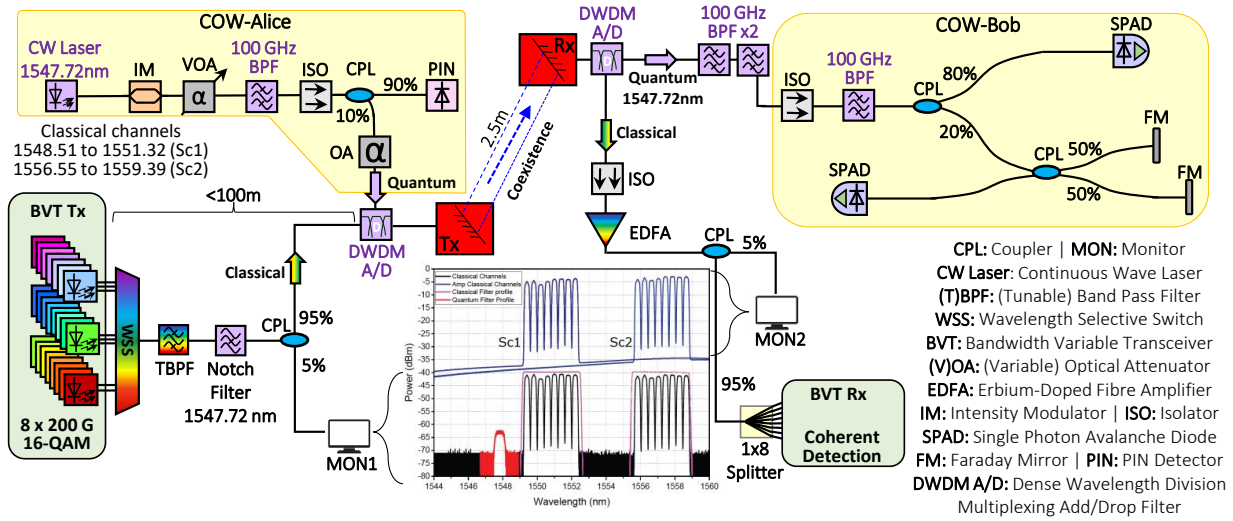

Fig. 6. Experimental testbed. Inset: Spectrum of the combined transmission of quantum and classical channels with optical filter profiles of both scenarios.

levels. A 95/5 coupler is used to monitor the amplified classical channel profile (blue channels in the inset Fig. 6). The 95% output port is connected to a 1x8 splitter separating the eight classical channels for coherent detection. A summary of main parameters of the testbed is shown in Table I.

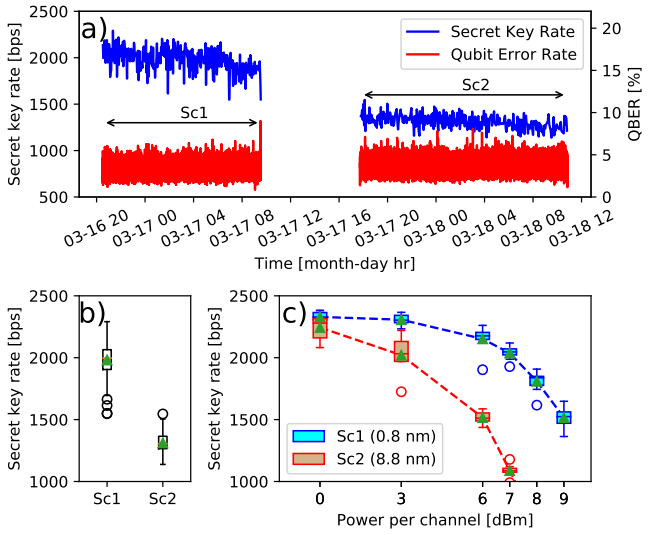

Fig. 7. Long term measurements of the QKD link operating in coexistence with 1.6 Tbit/s classical comms link in two different scenarios of spectral spacing. a) Data sets of the night from 16-03 to 17-03 with 100 GHz spectral spacing (Sc1) and from 17-03 to 18-03 with 1100 GHz spectral spacing (Sc2). b) Statistical representation of a). c) Secret key rate vs launch power per channel with the FWF terminals replaced with a 6 dB attenuator.

Due to the orders of magnitude difference in power between the QKD and the classical channels, Raman scattering caused by the classical channel degrades the QKD performance. Raman scattering is a non-linear optical effect and therefore has got a spectral response. In fibre optics both Stokes peaks of the Raman scattering can be found $\approx$ 1.1 THz around a 1550 nm communication channel [48]. Next to the spectral spacing, the launch power of the classical communication channels determine the amount Raman scattering [30]. Hence, two scenarios have been chosen to investigate the influence of channel spacing as shown in Fig. 6 and Tab. I. A spectral spacing of 100 GHz (0.8 nm, labeled "Sc1") means the quantum channel is placed in a Raman spectrum dip, whereas a spacing of 1.1 THz (8.8 nm, labeled "Sc2") means the quantum channel is placed at the Stokes peak causing additional crosstalk within the BPF filter bandwidth. Fig. 7a) and b) illustrate the long term stability of the pointing mirrors for both scenarios for at least 12 hours and with 7 dBm launch power per BVT channel. None of the classical communication channels was impaired at any time of observation. The measurement results for the QKD link clearly indicate the presence of Raman noise causing a reduction in secret key rate. The origin of the Raman scattering can be found in the <100 m fibre - connecting the BVT and WSS from another lab with the experimental setup. Fig. 7c) shows a set of measurements of the experimental testbed with the FWF terminals replaced by a 6 dB fixed attenuator. It can be seen that the launch power of the classical channels as well as the spectral spacing affect to the QKD channel impair the secret key rate. Furthermore, the measurement results for 7 dBm launch power co-align with the results presented in Fig. 7a) and b) proving the FWF terminals to be transparent for photons either associated with QKD, Raman noise or classical communication.

Finally, the robustness of the coexisting free-space link was tested against angular link misalignment in the presence of Raman noise (Sc2). Additional link losses were introduced by deliberately steering the receiver terminal off-axis by 0.021° as this steering angle has demonstrated a minimum impact on the QKD performance as shown in Fig. 5. That value of angular link misalignment did not impair the performance of any of the classical communication channels. The QKD measurement results are summarised in Fig. 8. It can be seen that the secret key rate increased by 44% compared to the on-axis steering position. Furthermore, the mean value of the QBER is reduced and the number of outliers representing high error rates are significantly reduced. The same observation can

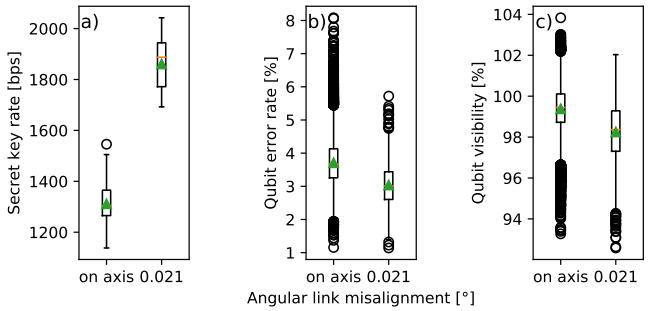

Fig. 8. Comparison between on axis steering and slightly off-axis steering in Sc2. All three key parameters of a QKD link are displayed.

be taken from the Qubit visibility: Even though the mean value is slightly reduced, the number of outliers representing lower Qubit visibility is significantly reduced. The main contributor of this behaviour is the change in insertion loss. The QKD channel tolerates the additional loss as demonstrated earlier. However, the Raman noise - and therefore the noise induced Qubit error counts - decrease accordingly with this increased loss. The combination of those two circumstances lead to an increased secret key rate at the given link misalignment despite the increased overall channel loss.

V. Conclusion

To the best of authors' knowledge, this paper presents the first experimental demonstration of the transmission of a COW-based DV-QKD channel coexisting with classical channels in free-space. The FWF terminal system presented allows for indoor QKD transmissions in a 200 lx environment free of performance penalties and for thorough investigation of the QKD performance. Pointing accuracy is key to maintain a free-space optical quantum link. However, the required pointing accuracy depends on the link budget provided by the QKD system, the insertion loss of the fibre-optical components and the distance covered between the terminals. Compared to previous Tbit/s FWF links over 2.5 m distance [34], the tracking accuracy needed for the QKD channel had to be refined by a factor of 10 due to tighter margins. The observed mean values of the secret key rates without coexistence, in coexistence in the Raman dip and at the Raman peak were 2.343 kbit/s, 1.996 kbit/s and 1.305 kbit/s, respectively. The coexistence of quantum and 1.6 Tbit/s classical data in free-space has been demonstrated highlighting the crucial role of curating the combined signal as Raman scattering generated in fibre optics impairs the QKD performance in free-space. This behaviour has implications towards the integration of the FWF terminals in PON architectures. However, the deliberate introduction of additional losses by angular misalignment demonstrated the potential to increase the secret key rate by 44% in the presence of Raman noise.

The tracking accuracy of the FWF terminal system will be further improved for automated operation with QKD links. When sufficiently accurate the FWF terminals could find applications in the fields of home access networks as part of an all-optical network and connecting quantum computers.

Acknowledgment

This work was funded by the European Union's Horizon 2020 research and innovation program under grant agreement No. 820474 (project UNIQORN) and agreement No. 761329 (project WORTECS); The UK EPSRC / UKNQTP via The Quantum Communications Hub (EP/T001011/1) and the UK EPSRC project COALESCE (EP/P003990/1). The authors would like to thank Rushikesh Deshmukh for support designing the FWF terminals.

References

[1] C. H. Bennett and G. Brassard, "Quantum Cryptography: Public key distribution and coin tossing," in *Proceedings of IEEE, International Conference on Computers, Systems and Signal Processing*. IEEE, 1984, pp. 175–179.

[2] T. Schmitt-Manderbach, H. Weier, M. Fürst, R. Ursin, F. Tiefenbacher, T. Scheidl, J. Perdigues, Z. Sodnik, C. Kurtsiefer, J. G. Rarity *et al.*, "Experimental demonstration of free-space decoy-state quantum key distribution over 144 km," *Physical Review Letters*, vol. 98, no. 1, p. 010504, 2007.

[3] J.-Y. Wang, B. Yang, S.-K. Liao, L. Zhang, Q. Shen, X.-F. Hu, J.-C. Wu, S.-J. Yang, H. Jiang, Y.-L. Tang *et al.*, "Direct and full-scale experimental verifications towards ground–satellite quantum key distribution," *Nature Photonics*, vol. 7, no. 5, pp. 387–393, 2013.

[4] S.-K. Liao, W.-Q. Cai, W.-Y. Liu, L. Zhang, Y. Li, J.-G. Ren, J. Yin, Q. Shen, Y. Cao, Z.-P. Li *et al.*, "Satellite-to-ground quantum key distribution," *Nature*, vol. 549, no. 7670, pp. 43–47, 2017.

[5] Z. Wang, R. Malaney, and B. Burnett, "Satellite-to-earth quantum key distribution via orbital angular momentum," *Physical Review Applied*, vol. 14, no. 6, p. 064031, 2020.

[6] L. Mazzarella, C. Lowe, D. Lowndes, S. K. Joshi, S. Greenland, D. McNeil, C. Mercury, M. Macdonald, J. Rarity, and D. K. L. Oi, "Quarc: quantum research cubesat—a constellation for quantum communication," *Cryptography*, vol. 4, no. 1, p. 7, 2020.

[7] M. Peev, C. Pacher, R. Alléaume, C. Barreiro, J. Bouda, W. Boxleitner, T. Debuisschert, E. Diamanti, M. Dianati, J. Dynes *et al.*, "The SECOQC quantum key distribution network in Vienna," *New Journal of Physics*, vol. 11, no. 7, p. 075001, 2009.

[8] M. Sasaki, M. Fujiwara, H. Ishizuka, W. Klaus, K. Wakui, M. Takeoka, S. Miki, T. Yamashita, Z. Wang, A. Tanaka *et al.*, "Field test of quantum key distribution in the Tokyo QKD Network," *Optics Express*, vol. 19, no. 11, pp. 10 387–10 409, 2011.

[9] D. Stucki, M. Legre, F. Buntschu, B. Clausen, N. Felber, N. Gisin, L. Henzen, P. Junod, G. Litzistorf, P. Monbaron *et al.*, "Long-term performance of the SwissQuantum quantum key distribution network in a field environment," *New Journal of Physics*, vol. 13, no. 12, p. 123001, 2011.

[10] S. Wang, W. Chen, Z.-Q. Yin, H.-W. Li, D.-Y. He, Y.-H. Li, Z. Zhou, X.-T. Song, F.-Y. Li, D. Wang *et al.*, "Field and long-term demonstration of a wide area quantum key distribution network," *Optics Express*, vol. 22, no. 18, pp. 21 739–21 756, 2014.

[11] T. A. Eriksson, T. Hirano, B. J. Puttnam, G. Rademacher, R. S. Luís, M. Fujiwara, R. Namiki, Y. Awaji, M. Takeoka, N. Wada *et al.*, "Wavelength division multiplexing of continuous variable quantum key distribution and 18.3 Tbit/s data channels," *Communications Physics*, vol. 2, no. 1, pp. 1–8, 2019.

[12] J.-s. Lai, X.-y. Lin, Y. Qian, L. Liu, W.-y. Zhao, and H.-y. Zhang, "Deployment-oriented integration of DV-QKD and 100G optical transmission system," in *Asia Communications and Photonics Conference*. Optical Society of America, 2019, pp. T2H–1.

[13] A. Bahrami, A. Lord, and T. Spiller, "Quantum key distribution integration with optical dense wavelength division multiplexing: a review," *IET Quantum Communication*, 2020.

[14] E. Hugues-Salas, O. Alia, R. Wang, K. Rajkumar, G. T. Kanellos, R. Nejabati, and D. Simeonidou, "11.2 Tb/s classical channel coexistence with DV-QKD over a 7-core multicore fiber," *Journal of Lightwave Technology*, vol. 38, no. 18, pp. 5064–5070, 2020.
[15] O. Alia, R. S. Tessinari, S. Bahrani, T. D. Bradley, H. Sakr, K. Harrington, J. Hayes, Y. Chen, P. Petropoulos, D. Richardson, F. Poletti, G. T. Kanellos, R. Nejabati, and D. Simeonidou, "Dv-qkd coexistence with 1.6 tbps classical channels over hollow core fibre," *Journal of Lightwave Technology*, vol. 40, no. 16, pp. 5522–5529, 2022.
[16] S. Wang, Z.-Q. Yin, D.-Y. He, W. Chen, R.-Q. Wang, P. Ye, Y. Zhou, G.-J. Fan-Yuan, F.-X. Wang, Y.-G. Zhu *et al.*, "Twin-field quantum key distribution over 830-km fibre," *Nature Photonics*, pp. 1–8, 2022.
[17] I. Choi, R. J. Young, and P. D. Townsend, "Quantum information to the home," *New Journal of Physics*, vol. 13, no. 6, p. 063039, 2011.
[18] B. Fröhlich, J. F. Dynes, M. Lucamarini, A. W. Sharpe, Z. Yuan, and A. J. Shields, "A quantum access network," *Nature*, vol. 501, no. 7465, pp. 69–72, 2013.
[19] S. K. Joshi, D. Aktas, S. Wengerowsky, M. Lončarić, S. P. Neumann, B. Liu, T. Scheidl, G. C. Lorenzo, Ž. Samec, L. Kling *et al.*, "A trusted node–free eight-user metropolitan quantum communication network," *Science Advances*, vol. 6, no. 36, p. eaba0959, 2020.
[20] C. Elliott, D. Pearson, and G. Troxel, "Quantum cryptography in practice," in *Proceedings of the 2003 Conference on Applications, Technologies, Architectures, and Protocols for Computer Communications*, 2003, pp. 227–238.
[21] I. Choi, R. J. Young, and P. D. Townsend, "Quantum key distribution on a 10Gb/s WDM-PON," *Optics Express*, vol. 18, no. 9, pp. 9600–9612, 2010.
[22] B.-X. Wang, S.-B. Tang, Y. Mao, W. Xu, M. Cheng, J. Zhang, T.-Y. Chen, and J.-W. Pan, "Practical quantum access network over a 10 Gbit/s Ethernet passive optical network," *Optics Express*, vol. 29, no. 23, pp. 38 582–38 590, 2021.
[23] O. Alia, R. S. Tessinari, E. Hugues-Salas, G. T. Kanellos, R. Nejabati, and D. Simeonidou, "Dynamic dv-qkd networking in trusted-node-free software-defined optical networks," *Journal of Lightwave Technology*, vol. 40, no. 17, pp. 5816–5824, 2022.
[24] G. Vest, M. Rau, L. Fuchs, G. Corrielli, H. Weier, S. Nauerth, A. Crespi, R. Osellame, and H. Weinfurter, "Design and evaluation of a handheld quantum key distribution sender module," *IEEE Journal of Selected Topics in Quantum Electronics*, vol. 21, no. 3, pp. 131–137, 2014.
[25] H. Chun, I. Choi, G. Faulkner, L. Clarke, B. Barber, G. George, C. Capon, A. Niskanen, J. Wabnig, and D. O`Brien, "Handheld free space quantum key distribution with dynamic motion compensation," *Optics Express*, vol. 25, no. 6, pp. 6784–6795, 2017.
[26] G. Vest, P. Freiwang, J. Luhn, T. Vogl, M. Rau, L. Knips, W. Rosenfeld, and H. Weinfurter, "Quantum key distribution with a hand-held sender unit," *Physical Review Applied*, vol. 18, no. 2, p. 024067, 2022.
[27] S. Nauerth, F. Moll, M. Rau, C. Fuchs, J. Horwath, S. Frick, and H. Weinfurter, "Air-to-ground quantum communication," *Nature Photonics*, vol. 7, no. 5, pp. 382–386, 2013.
[28] C. Quintana, P. Sibson, G. Erry, Y. Thueux, E. Kingston, T. Ismail, G. Faulkner, J. Kennard, K. Gebremicael, C. Clark *et al.*, "Low size, weight and power quantum key distribution system for small form unmanned aerial vehicles," in *Free-Space Laser Communications XXXI*, vol. 10910. International Society for Optics and Photonics, 2019, p. 1091014.
[29] A. T. Castillo, E. Eso, and R. Donaldson, "In-lab demonstration of coherent one-way protocol over free space with turbulence simulation," *Optics Express*, vol. 30, no. 7, pp. 11 671–11 683, 2022.
[30] J. F. Dynes, W. W. Tam, A. Plews, B. Fröhlich, A. W. Sharpe, M. Lucamarini, Z. Yuan, C. Radig, A. Straw, T. Edwards *et al.*, "Ultra-high bandwidth quantum secured data transmission," *Scientific Reports*, vol. 6, no. 1, pp. 1–6, 2016.
[31] A. Gomez, K. Shi, C. Quintana, M. Sato, G. Faulkner, B. C. Thomsen, and D. O'Brien, "Beyond 100-gb/s indoor wide field-of-view optical wireless communications," *IEEE Photonics Technology Letters*, vol. 27, no. 4, pp. 367–370, 2014.
[32] C. Oh, E. Tangdiongga, and A. Koonen, "Steerable pencil beams for multi-gbps indoor optical wireless communication," *Optics Letters*, vol. 39, no. 18, pp. 5427–5430, 2014.
[33] T. Koonen, F. Gomez-Agis, F. Huijskens, K. A. Mekonnen, Z. Cao, and E. Tangdiongga, "High-capacity optical wireless communication using two-dimensional ir beam steering," *Journal of Lightwave Technology*, vol. 36, no. 19, pp. 4486–4493, 2018.
[34] R. Singh, F. Feng, Y. Hong, G. Faulkner, R. Deshmukh, G. Vercasson, O. Bouchet, P. Petropoulos, and D. O'Brien, "Design and Characterisation of Terabit/s Capable Compact Localisation and Beam-Steering Terminals for Fiber-Wireless-Fiber Links," *Journal of Lightwave Technology*, vol. 38, no. 24, pp. 6817–6826, 2020.
[35] Y. Hong, F. Feng, K. R. Bottrill, N. Taengnoi, R. Singh, G. Faulkner, D. C. O'Brien, and P. Petropoulos, "Demonstration of 1Tbit/s WDM OWC with wavelength-transparent beam tracking-and-steering capability," *Optics Express*, vol. 29, no. 21, pp. 33 694–33 702, 2021.
[36] D. Lowndes, A. Schreier, D. O'Brien, and J. Rarity, "Characterising a handheld quantum key distribution system with emulated beam steering," in *Quantum Technology: Driving Commercialisation of an Enabling Science II*, vol. 11881. SPIE, 2021, pp. 9–13.
[37] O. Elmabrok, M. Ghalaii, and M. Razavi, "Quantum-classical access networks with embedded optical wireless links," *JOSA B*, vol. 35, no. 3, pp. 487–499, 2018.
[38] S. Bahrani, O. Elmabrok, G. C. Lorenzo, and M. Razavi, "Wavelength assignment in quantum access networks with hybrid wireless-fiber links," *JOSA B*, vol. 36, no. 3, pp. B99–B108, 2019.
[39] R. Donaldson, D. Kundys, A. Maccarone, R. Henderson, G. S. Buller, and A. Fedrizzi, "Towards combined quantum bit detection and spatial tracking using an arrayed single-photon sensor," *Optics Express*, vol. 29, no. 6, pp. 8181–8198, 2021.
[40] R. Singh, A. Schreier, G. Faulkner, and D. O'Brien, "Fiber-wireless-fiber terminals for optical wireless communication over multiple bands," in *2020 IEEE Photonics Conference (IPC)*. IEEE, 2020, pp. 1–2.
[41] S. Yuan and N. A. Riza, "General formula for coupling-loss characterization of single-mode fiber collimators by use of gradient-index rod lenses," *Applied Optics*, vol. 38, no. 15, pp. 3214–3222, 1999.
[42] IDQuantiqueSA, "Clavis3 qkd platform," https://www.idquantique.com/quantum-safe-security/products/clavis3-qkd-platform-rd/, May 2021.
[43] D. Stucki, C. Barreiro, S. Fasel, J.-D. Gautier, O. Gay, N. Gisin, R. Thew, Y. Thoma, P. Trinkler, F. Vannel *et al.*, "Continuous high speed coherent one-way quantum key distribution," *Optics Express*, vol. 17, no. 16, pp. 13 326–13 334, 2009.
[44] D. Stucki, N. Brunner, N. Gisin, V. Scarani, and H. Zbinden, "Fast and simple one-way quantum key distribution," *Applied Physics Letters*, vol. 87, no. 19, p. 194108, 2005.
[45] N. Gisin, S. Fasel, B. Kraus, H. Zbinden, and G. Ribordy, "Trojan-horse attacks on quantum-key-distribution systems," *Physical Review A*, vol. 73, no. 2, p. 022320, 2006.
[46] F. Engineering, "An open approach for switching, routing, and transport," https://engineering.fb.com/2016/11/01/connectivity/an-open-approach-for-switching-routing-and-transport/, Nov. 2016.
[47] Standard, "EN 60825-1: 2014—Safety of Laser Products," *Equipment Classification and Requirements*, 2014.
[48] K. Rottwitt, J. Bromage, and L. Leng, "Scaling the raman gain coefficient of optical fibers," in *2002 28TH European Conference on Optical Communication*, vol. 3. IEEE, 2002, pp. 1–2.